Liau and Chao *Earth, Planets and Space* (2017) 69:93
DOI 10.1186/s40623-017-0678-3

Earth, Planets and Space

FULL PAPER

Open Access

Variation of Antarctic circumpolar current and its intensification in relation to the southern annular mode detected in the time-variable gravity signals by GRACE satellite

Jen-Ru Liau[1,2] and Benjamin F. Chao[1*]

Abstract

The southern annular mode (SAM) in the atmosphere and the Antarctic circumpolar current (ACC) in the ocean play decisive roles in the climatic system of the mid- to high-latitude southern hemisphere. Using the time-variable gravity data from the GRACE satellite mission, we find the link between the space–time variabilities of the ACC and the SAM. We calculate the empirical orthogonal functions (EOF) of the non-seasonal ocean bottom pressure (OBP) field in the circum-Antarctic seas from the GRACE data for the period from 2003 to 2015. We find that the leading EOF mode of the non-seasonal OBP represents a unison OBP oscillation around Antarctica with time history closely in pace with that of the SAM Index with a high correlation of 0.77. This OBP variation gives rise to a variation in the geostrophic flow field; the result for the same EOF mode shows heightened variations in the zonal velocity that resides primarily in the eastern hemispheric portion of the ACC and coincided geographically with the southernmost boundary of the ACC's main stream. Confirming previous oceanographic studies, these geodetic satellite results provide independent information toward better understanding of the ACC–SAM process.

Keywords: Antarctic circumpolar current, Geostrophic balance, GRACE satellite, Southern annular mode

Introduction

Connecting the major Southern Hemisphere oceans, the *Antarctic circumpolar current* (ACC) plays a decisive role in the mid- to high-latitude SH climate and its variability (e.g., Nowlin and Klinck 1986; Olbers et al. 2004). The ACC is an eastward geostrophic flow manifesting as a zonal circulation (clockwise when viewed from above Antarctica) typically in the form of series of fronts and turbulent jets around the Antarctica continent (e.g., Rintoul et al. 2001; Olbers et al. 2004; Mayewski et al. 2009).

In much of the same region, the *southern annular mode* (SAM), also known as the Antarctic Oscillation, is the principal mode of meteorological variability that dominates the intraseasonal-to-interannual variability in the atmospheric wind, temperature and precipitation fields which, as a result, exhibit significant and widespread variabilities that follow the SAM (van den Broeke and van Lipzig 2004). The SAM-related atmospheric pressure gradient between the Antarctic low and the sub-Antarctic high modulates the strength of the westerlies. The strength variation of the SAM is customarily quantified by the *SAM Index*, defined as the leading principal component of the 700 hPa atmospheric geopotential height anomalies in the Antarctic region (e.g., Mo 2000).

It is known that the ACC transport depends on the eastward wind stress over the Southern Ocean (Thompson and Wallace 2000). For example, in the positive phase of the SAM, the region of the largest westerly surface wind stress shifts poleward giving rise to a poleward intensification of the ACC, which in turn enhances the equatorward Ekman transport across the ACC (Hall and Visbeck 2002). The negative SAM Index signifies the

*Correspondence: bfchao@earth.sinica.edu.tw
[1] Institute of Earth Sciences, Academia Sinica, Taipei, Taiwan, ROC
Full list of author information is available at the end of the article

opposite (Fig. 1). This response has been shown to hold on timescales from days and weeks (Aoki et al. 2003; Hughes et al. 2003) to years (Meredith et al. 2004). In addition, the ACC can show intrinsic variability independent of changes in wind forcing, through positive feedback between the generation of mesoscale eddies through baroclinic instability and the dynamics of the mean circulation (Hogg and Blundell 2006). That relationship has been demonstrated in situ across the Drake Passage based on bottom pressure and tide gauge records there (Meredith et al. 2011), and in an episode of anomalously high eddy kinetic energy (EKE) in the ACC via satellite altimeter data (Meredith and Hogg 2006).

Since its launch in 2002, the twin-satellite mission of the Gravity Recovery and Climate Experiment (GRACE) (Tapley et al. 2004) has been observing the time-variable gravity (TVG) data for the study of mass transports occurring on or in the Earth. In the oceans, the TVG signal magnitude is subdued relatively to that on land (e.g., Lombard et al. 2007; Chambers and Bonin 2012). For the ACC, Zlotnicki et al. (2007) used the GRACE TVG data then available to estimate the seasonal ACC transport variability in conjunction with other observations. Böning et al. (2010; see also Böning et al. 2008) compared 5 years of the early GRACE data with in situ observations and numerical model simulations and found the ACC correlation with the SAM. Boening et al. (2011) reported a GRACE finding of a record increase of ocean bottom pressure (OBP) in the southeast Pacific during late 2009. Bergmann and Dobslaw (2012) used the GRACE-based meridional OBP gradients to reveal significant correlations (>0.6) with the SAM on periods above 30 days, higher than those achieved with in situ observations and tide gauge data.

In this paper, we revisit the link between the space–time variability of the ACC and the SAM using the GRACE's TVG data for the period from 2003 to 2015, focusing on non-seasonal and broadband signals. We aim to study the spatiotemporal relationship of the ACC with the SAM in the entire region of the ACC around the Antarctica continent using the method of principal component analysis in the form of the empirical orthogonal functions (EOF). The circum-Antarctic oceans are in short of complete ocean-altimetry data given the 66° inclination of the TOPEX–Poseidon/Jason satellite orbits, and more importantly because of the extensive coverage of the winter sea ice over the studied region. By contrast, the GRACE TVG signals are indifferent to the state of the floating sea ice. Our study stands to confirm and strengthen what are already recognized in oceanographic results that are, however, less comprehensive in this region of hardship in observation. Our aim is to demonstrate the utility of the satellite TVG data in providing independent observations toward better understanding of the target oceanographic processes.

It should be emphasized at the outset that what we report in this paper are the *variations* in the ACC, not the ACC itself or its time-mean behavior. That is because the GRACE TVG data quantify large-scale mass redistributions referenced to the time-mean static geoid, in our case the time-mean "climatology" field. To study the latter would call for the determination of the ocean dynamic topography which in turn entails the ocean surface topography relative to the static geoid (for example from satellite altimetry observations) (e.g., Sánchez-Reales et al. 2012; Feng et al. 2013), work that is outside the scope of the present study.

Data and method

GRACE TVG data

We take the GRACE Level-2 Release-05 TVG data provided by the CSR (Center for Space Research, University of Texas), altogether 139 monthly global maps spanning a total of 12.5 years from January 2003 to July 2015. There are 16 missing months (June 2003, January 2011, June 2011, November 2011, December 2011, April 2012, May 2012, October 2012, March 2013, August 2013, September 2013, February 2014, July 2014, December 2014, May 2015 and June 2015) from the datasets; the moderate data gaps, however, pose no computational obstacles to our analysis which does not insist on equally spaced data. The TVG data, solved from the GRACE satellite orbit tracking, are provided in terms of spherical-harmonic Stokes coefficients that are suitable for representing data defined on the surface of a sphere. Assuming that the mass redistribution (that are of interest here) only occurs on the Earth surface (Wahr et al. 1998; Chao 2005, 2016) such as in the oceans, the TVG can be converted directly into the variation of OBP:

$$P(\theta,\,\lambda,\,t) = \frac{Rg\rho_{ave}}{3}\sum_{l=2}^{60}\frac{2l+1}{1+k_l'}\sum_{m=0}^{l}P_{lm}(\cos\theta) \times (\Delta C_{lm}(t)\cos m\lambda + \Delta S_{lm}(t)\sin m\lambda) \quad (1)$$

(Wahr et al. 2002; Bergmann and Dobslaw 2012), where $(\theta,\,\lambda)$ = (colatitudes, longitude), $R = 6378$ km, $g = 9.7983$ m/s^2 and $\rho_{ave} = 5517$ kg/m^3 are, respectively, the Earth's mean radius, mean surface gravitational acceleration and mean density, k_l' is the load Love number of degree l accounting for the Earth's elastic yielding effect under mass loading (Munk and Macdonald 1960) and P_{lm} is the normalized associated Legendre function of harmonic degree l and order m. One pascal (Pa = N/m^2) of the OBP corresponds to approximately 0.1 mm of equivalent water thickness.

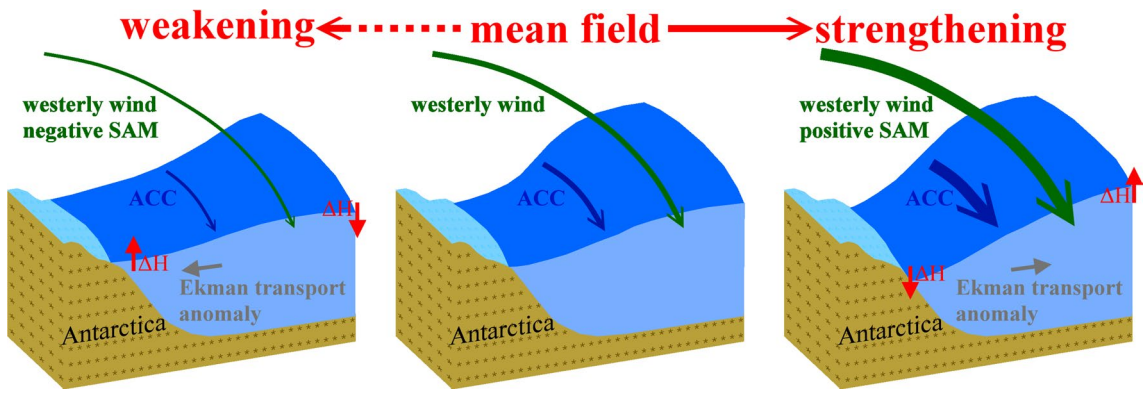

Fig. 1 Schematic depiction of the circum-Antarctic ringed geometry and the variability of the ACC in relation to the SAM over the Southern Ocean. A positive SAM Index (*on the right panel*) means the stronger westerly wind, the faster ACC, the Ekman transport anomaly moving toward the equator, and the sea level increasing (*decreasing*) away from (*toward*) the Antarctica. A negative SAM Index (*on the left panel*) signifies the opposite

The parameters ΔC_{lm} and ΔS_{lm} are the monthly *variation* of Stokes coefficients provided up to degree and order 60. The corresponding spatial resolution is ~300 km nominally, but becomes favorably finer poleward to better than 200 km given the GRACE satellite's near-polar orbit configuration. Our study area is the southern plus sub-Antarctic oceans south of 45°S, excluding 3° off the Antarctica coasts to avoid land signal leakages. To circumvent the numerical awkwardness of the "shrinking" spacing toward the poles in the conventional latitude/longitude gridding that calls for artificial area weighting of data (such as by the factor $\cos\theta$ or alternatively its square root in computing the EOF), we resample the GRACE data into a uniform reduced Gaussian grid (N80) at nominal spacing of 125 km with altogether 5196 grid points to be input to the EOF process.

The two TVG constituent datasets are involved: The GAD dataset is one of the Atmosphere and Ocean Dealiasing Level-1B products utilized in the GRACE data pre-processing to avoid aliasing errors from atmospheric and oceanic signals higher in frequency than monthly. Specifically, it is the part of the non-tidal OBP as modeled by state-of-the-art atmosphere–ocean circulation models, including both barotropic and baroclinic effects. The atmospheric contribution is zeroed out over land in the GAD, and the ocean–atmosphere inverted barometer effect is included as appropriate for the spatial and temporal scales of concern. The main dataset GSM is the GRACE-observed TVG upon the removal of the GAD (Flechtner 2007). In our present work, we add back the GAD to the GSM, forming the dataset the GAD+GSM thus to restore the "true" GRACE-observed OBP field.

As is a common practice in the GRACE data processing, the $l = 2$ Stokes coefficient C_{20} data are replaced with those from the satellite laser ranging which is more reliable than the GRACE C_{20} (Cheng and Ries 2008) and we apply two spatial filters sequentially to reduce the N–S striping and high-wave-number noises in the GRACE GSM data, namely a decorrelation filter using the same empirical parameters as their result (Duan et al. 2009) and an anisotropic fan filter at 300 km radius (Zhang et al. 2009). We do the same filtering on the GAD for consistency.

EOF of non-seasonal signals

As stated, we are interested in the broadband, intraseasonal–interannual variations minus the strong seasonality. To remove the non-target signals, we model the OBP time series processed above at any given grid point as:

$$P(t) = a + bt + ct^2 + \alpha_1 \sin\omega t + \beta_1 \cos\omega t + \alpha_2 \sin 2\omega t + \beta_2 \cos 2\omega t + \text{“residual } \Delta P(t)\text{”}. \quad (2)$$

The polynomial accounts for a quadratic trend (including the mean), and the sinusoidal terms [where $\omega = 2\pi/(365.26 \text{ days})$] represent the annual and semi-annual seasonal signals. The coefficients are then estimated via linear least-squares regression, and the resultant analytical terms subtracted to yield the non-seasonal residual $\Delta P(t)$. Note that removing the quadratic term practically removes the dominant trending signals of land-ice mass depletion/growth on the Antarctica (including their leakages to the ocean area), as well as possible non-surficial effect of the post-glacier rebound TVG so that the conversion of the TVG to the OBP (Eq. 1) is further justified.

The three $l = 1$ Stokes coefficients corresponding to the geocenter motion are not included in the GRCAE data. Swenson et al. (2008) estimated that the geocenter has maximum annual amplitude of about 14 mm, while the non-seasonal standard deviation is much less at

~0.9 mm. The net regional variability within the studied area is a few times smaller still (for example, cos60°–cos45° = 0.16 across the latitude range). Such small variation is negligible compared to our detected signals of upwards of 10 mm.

The residual $\Delta P(t)$ anomaly from all grid points in the target region is then input to the EOF solutions (e.g., Preisendorfer and Mobley 1988; Hannachi et al. 2007). The EOF decomposes a spatiotemporal dataset into orthogonal standing-wave oscillations, or modes. Each mode consists of a spatial pattern multiplied by the corresponding temporal variability delimited with the target region and time span. In the following figures, we present the leading EOF mode solutions (of the largest eigenvalue) for the residual OBP anomaly $\Delta P(t)$; these leading modes are found to account for as much as 31–35% of the total variance in all cases. Note that the time series are normalized w.r.t. its standard deviation, so that the spatial pattern manifests the actual amplitude of the target physical quantity, in the present case the OBP variation in the unit of Pa.

Results

EOF of OBP

Figure 2a shows the leading EOF mode of the residual OBP around the Antarctica from the GAD field, the (processed) atmosphere–ocean general circulation model output. Its spatial pattern naturally has oscillating patches typical of the SAM as would be expected, with slight differences merely because of our exclusion of the land-area atmospheric signals and the data filtering we have applied. The corresponding time series correlates well with the SAM Index (with a linear correlation coefficient of 0.47), not surprisingly because they originate from similar meteorological products as noted above. As such, this correlation does not have anything to do with the GRACE observations *per se*.

Figure 2b, on the other hand, shows the leading EOF mode of the residual OBP $\Delta P(t)$ from the GRACE GSM data. It displays a quasi-annular band surrounding and abutting the Antarctica continent, which undergoes a unison variation. It should be pointed out that this variation, controlling the entire ocean area where the ACC resides, represents one dominant meteorological signal that is actually not captured by the present atmosphere–ocean general circulation models (Atmosphere and Ocean De-aliasing Level-1B products adopted by the GRACE project to yield the GAD data and removed from the GRACE observations as stated). The peak-to-peak amplitude seen here is up to ~400 Pa, equivalent to ~40 mm of water column thickness, which are actually subdued values after our heavy filtering (and being satellite-averaged in both space and time to begin with). High correlation is again found between the EOF time series and the SAM Index: The correlation coefficient is 0.66 at zero time shifts, far exceeding, say, the 0.1% significant level of 0.27 given the pertinent degree of freedom of the broadband GSM data.

When combined (as explained above), the non-seasonal $\Delta P(t)$ of the GAD+GSM data yields the leading EOF mode shown in Fig. 2c. Now one sees an EOF pattern that is essentially the sum of the EOF patterns of the two constituents, that is, the sum of Fig. 2a, b. Upon a moment of reflection, this is recognized to be a direct consequence of the similarity in the time history in Fig. 2a, b, here both being highly correlated with the SAM. The corresponding time series has an even stronger correlation with the SAM Index, now as high as 0.77. No significant correlation is seen in the other higher EOF mode time series with the SAM Index, see Additional file 1 (In passing, we have also done the same for the dataset GAC+GSM, where the GAC is just like the GAD but not excluding the land areas. Essentially, the same correlation patterns emerge despite the mixing of the land atmospheric contribution that is actually outside the interest here.)

Figure 2c thus shows that the OBP over the entire annular area surrounding the Antarctica oscillates closely in pace with the SAM, in such a way that during the time when the SAM Index is positive, the OBP there is depressed (shown in blue) and that of the outer areas rises in patches correspondingly, giving rise to a steeper N–S gradient (see Fig. 1); the reverse is true when the SAM Index is negative.

Derived geostrophic current

At a large scale, an OBP gradient gives rise to a horizontal geostrophic current. So do their variations, i.e., an OBP gradient variation gives rise to a geostrophic current variation, because the geostrophic balance between the pressure gradient and flow is a linear relation. Here we adopt the leading EOF mode of the GAD+GSM OBP variation found above in Fig. 2c and calculate the corresponding geostrophic current variation for the ACC around the Antarctica. Specifically, the geostrophic equation governing the variation of the horizontal zonal component Δu (positive for eastward) and meridional component Δv (positive for northward) of the flow velocity accompanying the OBP variation ΔP is:

$$\Delta u = -\frac{1}{\rho_w f}\frac{\partial \Delta P}{\partial y},\ \Delta v = \frac{1}{\rho_w f}\frac{\partial \Delta P}{\partial x} \tag{3}$$

where Δ denotes temporal change, $\rho_w = 1028$ kg/m^3 is the reference seawater density and $f = 2\Omega^*\sin(latitude)$ is the Coriolis parameter with $\Omega = 7.2921 \times 10^{-5}$ rad/s being the Earth's rotation rate. Since the spatial gradient

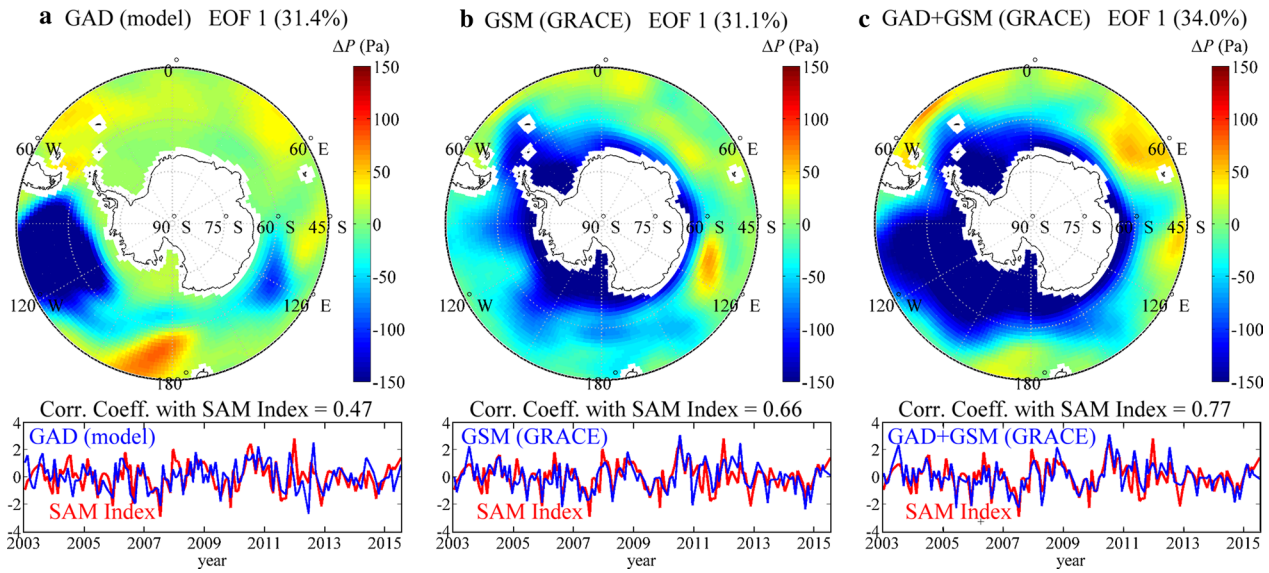

Fig. 2 The leading EOF mode solutions of the non-seasonal OBP from the GRACE datasets, where the spatial pattern shows the amplitude of fluctuation (with positive or negative polarity) at each location according to the corresponding time history, for the GRACE datasets of: **a** the GAD; **b** the GSM; and **c** the GAD+GSM. The spatial pattern is manifested as the OBP variation in unit of Pa; the time series (the *blue curves*) are normalized and compared with the SAM Index (the *red curve*)

is performed directly upon the EOF spatial patterns of Fig. 2c, the corresponding time history stays the same as in Fig. 2c. Note in passing that the geostrophic calculation can alternatively be done *prior to* the EOF analysis from the original GRACE datasets, coefficient by Stokes coefficient followed by summation (Wahr et al. 2002); the results would be the same as all the operations involved are linear.

Physically, the non-seasonal OBP ΔP field comprises two parts: A barotropic contribution $\rho_w g \Delta\eta$ from the dynamic height $\Delta\eta$ at the sea surface (as the mean field is removed), plus a baroclinic contribution from the variation in the internal steric pressure $g\int_{-h}^{0}\Delta\rho dz$ where h is the ocean depth of the field point and $\Delta\rho$ is the depth-dependent density perturbation of seawater dictated by the temperature and salinity. If one simplistically assumes a level of no motion at certain depth exceeding the typical depth of the ACC, then an effective depth can be defined for the flow field, and Δu and Δv reflect the depth-averaged variation of the geostrophic flow over the water column above the effective depth. If the variation of the baroclinic portion can be neglected, then Δu and Δv would be uniform in the water column and equal to the variation of the surface geostrophic flow. There is no feasible way to distinguish the two scenarios solely from the GRACE TVG data.

However, the following suggests that our leading EOF mode has indeed solved for the barotropic behavior of the ACC. Meredith and Hogg (2006) found that the SAM leads the EKE of the ACC by 1.5–2 years and proposed that the enhanced winds associated with an increasing SAM act to tilt isopycnals, which in turn increases the baroclinic instability. This mechanism is known as eddy saturation (Straub 1993). However, such phase difference is not evident in the cross-correlation functions of the leading EOF mode time series with the SAM Index which is shown in Fig. 3 and shows the peak correlation coefficient of 0.77 where the single prominent peak is at zero time shift. Moreover, the fact that the ACC variation keeps close pace with the SAM can be construed as evidence pronouncing that the influence largely originates from the surface by barotropic processes, as opposed to the baroclinic processes. By the same token, according to Eq. 3 the variation Δu translates into the variation in the N–S steepness of the circum-Antarctic gradient in the barotropic sea surface height.

The spatial pattern of the zonal component anomaly Δu thus derived is plotted in Fig. 4a. It exhibits a clear circum-Antarctic ringed pattern that represents the fluctuating Δu in a temporally unison manner. In particular, the main half-ring of the maximum Δu resides in the eastern hemisphere and coincides with the southernmost boundary of the main stream of the ACC. Here we re-emphasize that what the GRACE TVG data see here is the Δu variation in reference to the time-mean current field, not the u field itself. The peak-to-peak fluctuations of Δu in Fig. 4a are on the order of 5-10 mm/s, which, again, are numerically subdued values upon the smoothing and

filtering of the GRACE data as described above. The high correlation of the associated time series with the SAM (being of course the same as Fig. 2c) means the following: When the SAM Index is positive, the geostrophic circum-Antarctic Δu increases in near proportionality to the SAM Index and makes the zonal velocity faster than its time-mean value. The reverse happens when the SAM Index is negative.

In parallel, the rather weak signals in the meridional component Δv are plotted in Fig. 5a. We mention in passing that the combination of Δu and Δv suggests the presence of variations in the Ross Gyre also in pace with the SAM, whereas any more detailed study of it would entail, for instance, dedicated the regional EOF analysis which is beyond the scope here.

Decadal change

It has long been noted (e.g., Marshall 2003; Böning et al. 2008; Thompson et al. 2011; Frankcombe et al. 2013; Abram et al. 2014) that the SAM has seen gentle strengthening and poleward shift in the westerly wind field. This relatively long-term change over the course of the past few decades is attributed to an increasing atmospheric concentration of ozone-depleting and greenhouse gases. However, our present analysis cannot tell such trend signals because the linear terms have already been removed from our OBP data, and also because the GRACE timespan is too short. Nevertheless, we will attempt to see whether the GRACE data shed any light on the decadal variability of the coupled atmosphere–ocean system. We calculate the EOF for the GAD+GSM OBP anomaly in the same manner as above but separated into two ~7-year time segments: January 2003–December 2009 and January 2009–July 2015. Figure 4b, c shows the variability of Δu for the first and later halves and Fig. 5b, c for Δv, where we see the high correlation with the SAM prevails throughout. Comparing Fig. 4b, c, a strong variability of the anomaly Δu is evident, namely a clockwise shift of the most intensive portion of the ACC Δu *variation* along the whole eastern hemispheric coast.

To highlight this overall behavior change of Δu over the two time segments, we plot in Fig. 4d the Δu profiles along three chosen meridian cross sections of the EOF pattern for the two timespans separately, profiles AA′, BB′ and CC′ along longitudes 45°E, 90°E and 135°E, respectively, in the eastern hemisphere. While not much change is seen along AA′ between the two 7-year half-timespans, the variation Δu along BB′ and CC′ in the later half-timespan differs significantly relative to the first half, there of the peak Δu fluctuation between 60-65°S increases from about ± 2 to ± 4 mm/s. The change happens along much of the eastern hemispheric coast, most intensively in the "fourth quadrant" (in Fig. 4b) where

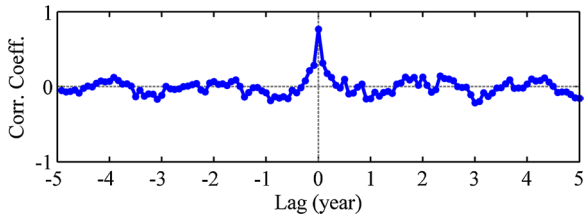

Fig. 3 The cross-correlation function as a function of time shift between the first EOF time series of the non-seasonal OBP from the GRACE GAD+GSM dataset and the SAM Index

the maximum variation Δu coincides with the southern or poleward rim of the ACC's main stream. As such, the positive/negative fluctuation of the ACC became more intense in pace with the SAM within latitude ~55–65°S during the course of the GRACE observation. This phenomenon presumably coexists with and is superimposed upon the findings of the significant trend in the ACC transport (Makowski et al. 2015).

Further discussion and concluding remarks

We find from the GRACE TVG data strong overall correlations between the ACC and the SAM. The method of the EOF proves to be highly efficient in extracting the spatiotemporal variability. Keeping close pace with the variation of the SAM, the variation in the zonal (eastward) geostrophic flow of the ACC derived from the OBP EOF solution is found to exhibit an obviously enhanced fluctuation in the southern ACC on the order of a few mm/s during the past decade. In this study, our results show that the anomalies are found in the area coinciding with the southernmost boundary of the ACC's main stream, close to the upwelling of the Antarctic Divergence in the Southern ACC Front. For example, Aoki et al. (2003) reported a slight warming over three decades at depths of 200–900 m in a region around 70°E, 62°S, suggesting that the Southern ACC Front had shifted southward. Our findings shed further light on this scenario. By contrast, Shao et al. (2015) found the correlation of the frontal positions with changing atmospheric forcing related to the SAM which is noisy, and Chapman (2017) found no statistically significant frontal displacements in the south of Australia with changing SAM. The root of this discrepancy is presently unclear.

Past studies have reported correlations between the OBP and the SAM in the mid- to high-latitude Southern Hemisphere in various case studies pertaining to certain specific situations in space and in time (e.g., Meredith et al. 2004; Zlotnicki et al. 2007; Böning et al. 2010; Bergmann and Dobslaw 2012; Makowski et al. 2015). In particular, Böning et al. (2010) have obtained the EOF solutions and reported high correlation between the

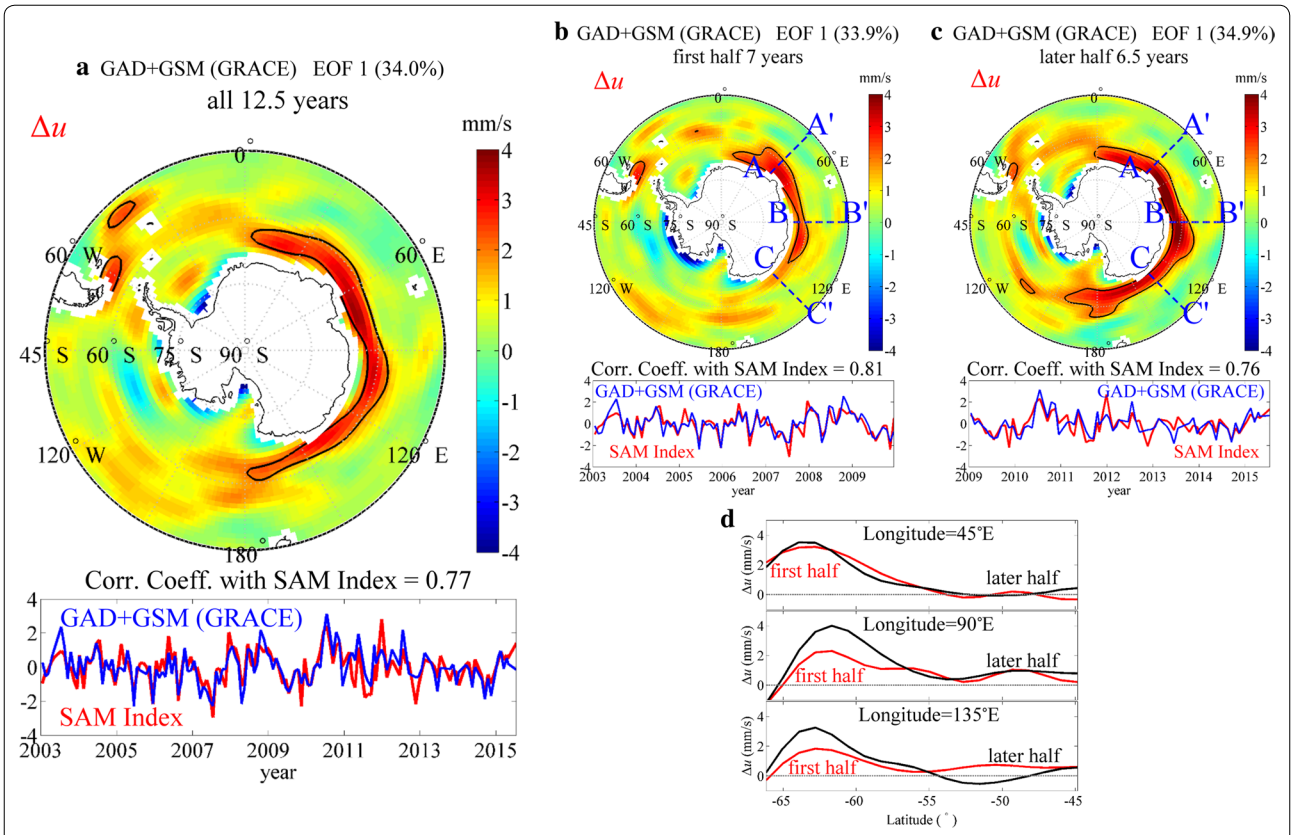

Fig. 4 **a** Variation of the zonal component (*positive for eastward*) of the geostrophic flow Δ*u* derived from the leading EOF mode of the non-seasonal OBP field in Fig. 2c, 2003–2015. **b** and **c** are the same as **a** but for two sub-timespans, January 2003–December 2009 and January 2009–July 2015, respectively. The *thick contours* denote ±2 mm/s of fluctuation. **d** The *red curves* are the Δ*u* profiles along cross sections *AA*′, *BB*′ and *CC*′ in the eastern hemisphere in **b**, and the *black curves* are the same w.r.t. **c**, showing the poleward intensification of the *ringed pattern* of Δ*u* along *BB*′ and *CC*′

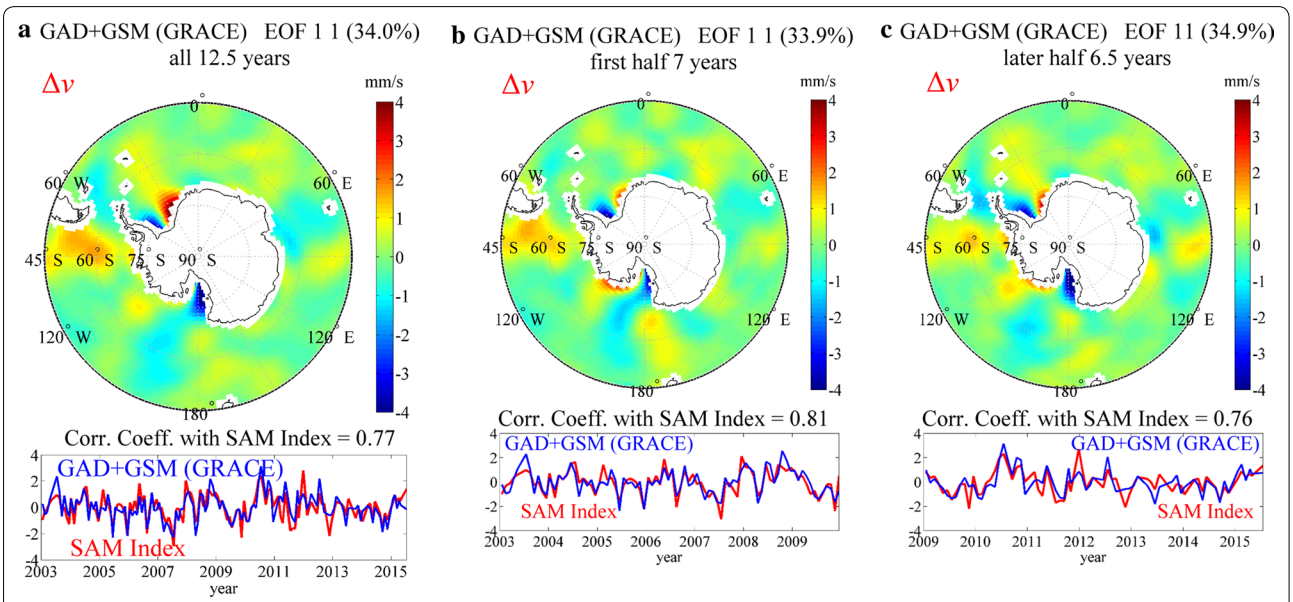

Fig. 5 Same as Fig. 4a–c, but for the variation of the meridional component (*positive for northward*) of the geostrophic flow Δ*v*

SAM and the GRACE TVG data. Our analysis essentially follows the same approach in processing the GRACE TVG observations. Nevertheless, using the improved GRACE data (Release-05) which are over twice longer in timespan, we are able to obtain a much clearer and definitive set of results for the EOF solutions than previous studies. For one thing, the present results suffer considerably less from the striping noise. More importantly, our analysis is done on the non-seasonal signals that are more conducive to geophysical interpretation in terms of the broadband correlation between the SAM and the GRACE observations. Furthermore, we have extended the calculated EOF to the variation in the geostrophic ACC flow and detected evidence for a change over the timespan of the GRACE observation of 12.5 years. The GRACE TVG data have been used extensively in monitoring mass redistribution phenomena on land and, to a lesser extent but increasingly, over oceans, in particular in studying ocean dynamics as exemplified in the present analysis of the ACC variations. Parallel studies have been conducted for major ocean currents, for example the correlation found with the GRACE bottom pressure data and the Kuroshio Extension System Study array (Park et al. 2008). For the Gulf Stream, the sensitivity of the GRACE observation is sufficient to record interannual transport anomalies in the Atlantic Meridional Overturning Circulation components (Landerer et al. 2015). The EOF analysis for the Arctic Ocean has also revealed a mass change along the Siberian shelves driven by surface Ekman transport associated with the Arctic Oscillation (Peralta-Ferriz et al. 2014). It would be natural to anticipate further applications of the satellite TVG data in these areas.

Additional file

Additional file 1. The higher EOF mode solutions of the non-seasonal OBP (ΔP) from the GRACE GAD+GSM dataset. The spatial pattern shows the amplitude of fluctuation (with positive or negative polarity) at each location according to the corresponding time history and is manifested as the OBP variation in unit of Pa. The time series (the blue curves) are normalized and compared with the SAM Index (the red curve). For each mode, we also show the percentage of total variance. For the cross-correlation function, positive lags mean that the SAM Index leads the EOF mode time series.

Abbreviations

ACC: Antarctic circumpolar current; EKE: eddy kinetic energy; EOF: empirical orthogonal functions; GRACE: Gravity Recovery and Climate Experiment; OBP: ocean bottom pressure; SAM: southern annular mode; TVG: time-variable gravity.

Authors' contributions

JRL and BFC developed the ideas that led to this paper, discussed the results and wrote the paper; JRL analyzed the data and generated the figures. All authors read and approved the final manuscript.

Author details

[1] Institute of Earth Sciences, Academia Sinica, Taipei, Taiwan, ROC. [2] Department of Earth Sciences, National Central University, Taoyuan City, Taiwan, ROC.

Acknowledgements

We are grateful to Yun-Hao Wu for discussions and K. Katsumata and W. Feng for useful information, the anonymous reviewers for their detailed and insightful comments to the manuscript. We particularly thank the assistance of the summer intern students Ya-Min Yang, Ya-Ting Tsui and Wan-Hsin Yang. The TVG data were available from the GRACE Project and the Center for Space Research, University of Texas. This work is supported by the Ministry of Science and Technology of Taiwan via Grants #103-2116-M-001-024, 104-2116-M-001-006 and 105-2116-M-001-016.

Competing interests

The authors declare that they have no competing interests.

Publisher's Note

Received: 25 January 2017 Accepted: 27 June 2017
Published online: 06 July 2017

References

Abram NJ, Mulvaney R, Vimeux F, Phipps SJ, Turner J, England MH (2014) Evolution of the Southern Annular Mode during the past millennium. Nat Clim Chang 4:564–569. doi:10.1038/nclimate2235

Aoki S, Yoritaka M, Masuyama A (2003) Multidecadal warming of subsurface temperature in the Indian sector of the Southern Ocean. J Geophys Res 108(C4):8081. doi:10.1029/2000JC000307

Bergmann I, Dobslaw H (2012) Short-term transport variability of the Antarctic Circumpolar Current from satellite gravity observations. J Geophys Res 117:C05044. doi:10.1029/2012JC007872

Boening C, Lee T, Zlotnicki V (2011) A record-high ocean bottom pressure in the South Pacific observed by GRACE. Geophys Res Lett 38(4):L04602. doi:10.1029/2010GL046013

Böning CW, Dispert A, Visbeck M, Rintoul SR, Schwarzkopf FU (2008) The response of the Antarctic Circumpolar Current to recent climate change. Nat Geosci 1:864–869. doi:10.1038/ngeo362

Böning C, Timmermann R, Danilov S, Schröter J (2010) Antarctic circumpolar current transport variability in GRACE gravity solutions and numerical ocean model simulations. In: Gruber T, Güntner A, Mandea M, Rothacher M, Schöne T, Wickert J, Flechtner FM (eds) System earth via geodetic-geophysical space techniques advanced technologies in earth sciences. Springer, Berlin, pp 187–199. doi:10.1007/978-3-642-10228-8

Chambers DP, Bonin JA (2012) Evaluation of release-05 GRACE time-variable gravity coefficients over the ocean. Ocean Sci 8(5):859–868. doi:10.5194/os-8-859-2012

Chao BF (2005) On inversion for mass distribution from global (time-variable) gravity field. J Geodynamics 39(3):223–230. doi:10.1016/j.jog.2004.11.001

Chao BF (2016) Caveats on the equivalent-water-thickness and surface mascon solutions derived from the GRACE satellite-observed time-variable gravity. J Geod 90(9):807–813. doi:10.1007/s00190-016-0912-y

Chapman CC (2017) New perspectives on frontal variability in the Southern Ocean. J Phys Oceanogr 47(5):1151–1168. doi:10.1175/JPO-D-16-0222.1

Cheng MK, Ries J (2008) Monthly estimates of C20 from 5 SLR satellites based on GRACE RL05 models. In: GRACE technical note #07. Center for Space Research Publication, University of Texas at Austin. ftp://podaac.jpl.nasa.gov/allData/grace/docs/TN-07_C20_SLR.txt

Duan XJ, Guo JY, Shum CK, van der Wal W (2009) On the postprocessing removal of correlated errors in GRACE temperal gravity field solutions. J Geod 83(11):1095–1106. doi:10.1007/s00190-009-0327-0

Feng G, Jin S, Reales JMS (2013) Antarctic circumpolar current from satellite gravimetric models ITG-GRACE2010, GOCE-TIM3 and satellite altimetry. J Geodyn 72:72–80. doi:10.1016/j.jog.2013.08.005

Flechtner F (2007) AOD1B Product Description Document for Product Releases 01 to 04. GRACE Rev 3(1):327–750
Frankcombe LM, Spence P, Hogg AMcC, England MH, Griffies SM (2013) Sea level changes forced by Southern Ocean winds. Geophys Res Lett 40(21):5710–5715. doi:10.1002/2013GL058104
Hall A, Visbeck M (2002) Synchronous variability in the Southern Hemisphere atmosphere, sea ice, and ocean resulting from the Annular Mode. J Clim 15:3043–3057. doi:10.1175/1520-0442(2002)015<3043:SVITSH>2.0.CO;2
Hannachi A, Jolliffe IT, Stephenson DB (2007) Review empirical orthogonal functions and related techniques in atmospheric science: a review. Int J Climatol 27(9):1119–1152. doi:10.1002/joc.1499
Hogg AMcC, Blundell JR (2006) Interdecadal variability of the Southern Ocean. J Phys Oceanogr 36:1626–1645. doi:10.1175/JPO2934.1
Hughes CW, Woodworth PL, Meredith MP, Stepanov V, Whitworth T, Pyne AR (2003) Coherence of Antarctic sea levels, Southern Hemisphere Annular Mode, and flow through Drake Passage. Geophys Res Lett 30(9):1464. doi :10.1029/2003GL017240
Landerer FW, Wiese DN, Bentel K, Boening C, Watkins MM (2015) North Atlantic meridional overturning circulation variations from GRACE ocean bottom pressure anomalies. Geophys Res Lett 42:8114–8121. doi:10.1002/2015GL065730
Lombard A, Garcia D, Ramillien G, Cazenave A, Biancale R, Lemoine JM, Flechtner F, Schmidt R, Ishii M (2007) Estimation of steric sea level variations from combined GRACE and Jason-1 data. Earth Planet Sci Lett 254(1–2):194–202. doi:10.1016/j.epsl.2006.11.035
Makowski JK, Chambers DP, Bonin JA (2015) Using ocean bottom pressure from the gravity recovery and climate experiment (GRACE) to estimate transport variability in the southern Indian Ocean. J Geophys Res Oceans 120(6):4245–4259. doi:10.1002/2014JC010575
Marshall GJ (2003) Trends in the Southern Annular Mode from observations and reanalyses. J Clim 16:4134–4143. doi:10.1175/1520-0442(2003)016<4134:TITSAM>2.0.CO;2
Mayewski PA, Meredith MP, Summerhayes CP, Turner J, Worby A, Barrett PJ, Casassa G, Bertler NAN, Bracegirdle T, Naveira Garabato AC, Bromwich D, Campbell H, Hamilton GS, Lyons WB, Maasch KA, Aoki S, Xiao C, van Ommen Tas (2009) State of the Antarctic and Southern Ocean climate system. Rev Geophys 47:RG1003. doi:10.1029/2007RG000231
Meredith MP, Hogg AMcC (2006) Circumpolar response of Southern Ocean eddy activity to a change in the Southern Annular Mode. Geophys Res Lett 33(16):L16608. doi:10.1029/2006GL026499
Meredith M, Woodworth P, Hughes C, Stepanov V (2004) Changes in the ocean transport through Drake Passage during the 1980s and 1990s, forced by changes in the Southern Annular Mode. Geophys Res Lett 31(21):L21305. doi:10.1029/2004GL021169
Meredith MP, Woodworth PL, Chereskin TK, Marshall DP, Allison LC, Bigg GR, Donohue K, Heywood KJ, Hughes CW, Hibbert A, Hogg AMcC, Johnson HL, Jullion L, King BA, Leach H, Lenn Y, Morales Maqueda MA, Munday DR, Naveira Garabato AC, Provost C, Sprintall J-B (2011) Sustained monitoring of the Southern Ocean at Drake Passage: past achievements and future priorities. Rev Geophys 49(4):RG4005. doi:10.1029/2010RG000348
Mo KC (2000) Relationships between low-frequency variability in the Southern Hemisphere and sea surface temperature anomalies. J Clim 13:3599–3610. doi:10.1175/1520-0442(2000)013<3599:RBLFVI>2.0.CO;2
Munk WH, MacDonald GJF (1960) The rotation of the earth: a geophysical discussion. Cambridge University Press, New York, p 323
Nowlin WD Jr, Klinck JM (1986) The physics of the Antarctic circumpolar current. Rev Geophys 24(3):469–491. doi:10.1029/RG024i003p00469
Olbers D, Borowski D, Völker C, Wölff JO (2004) The dynamical balance, transport and circulation of the Antarctic circumpolar current. Antarct Sci 16(4):439–470. doi:10.1017/S0954102004002251
Park JH, Watts DR, Donohue KA, Jayne SR (2008) A comparison of in situ bottom pressurearray measurements with GRACE estimates in the Kuroshio Extension. Geophys Res Lett 35:L17601. doi:10.1029/2008GL034778
Peralta-Ferriz C, Morison JH, Wallace JM, Bonin JA, Zhang J (2014) Arctic ocean circulation patterns revealed by GRACE. J Clim 27(4):1445–1468. doi:10.1175/JCLI-D-13-00013.1
Preisendorfer RW, Mobley CD (1988) Principal component analysis in meteorology and oceanography. Elsevier, Amsterdam. ISBN 0444430148
Rintoul SR, Hughes C, Olbers D (2001) The Antarctic Circumpolar Current system. In: Siedler G, Church J, Gould J (eds) Ocean circulation and climate. Academic Press, London, pp 271–302. ISBN 0126413517
Sánchez-Reales JM, Vigo I, Jin SG, Chao BF (2012) Global surface geostrophic ocean currents derived from satellite altimetry and GOCE geoid. Mar Geod 35(1):175–189. doi:10.1080/01490419.2012.718696
Shao AE, Gille ST, Mecking S, Thompson L (2015) Properties of the Subantarctic Front and Polar Front from the skewness of sea level anomaly. J Geophys Res Oceans 120:5179–5193. doi:10.1002/2015JC010723
Straub DN (1993) On the transport and angular momentum balance of channel models of the Antarctic circumpolar current. J Phys Oceanogr 23:776–782. doi:10.1175/1520-0485(1993)023<0776:OTTAAM>2.0.CO;2
Swenson S, Chambers D, Wahr J (2008) Estimating geocenter variations from a combination of GRACE and ocean model output. J Geophys Res 113:B08410. doi:10.1029/2007JB005338
Tapley BD, Bettadpur S, Watkins M, Reigber C (2004) The gravity recovery and climate experiment: mission overview and early results. Geophys Res Lett 31(9):L09607. doi:10.1029/2004GL019779
Thompson DWJ, Wallace JM (2000) Annular modes in the extratropical circulation. Part I: month-to-month variability. J Clim 13:1000–1016. doi:10.1175/1520-0442(2000)013<1000:AMITEC>2.0.CO;2
Thompson DWJ, Solomon S, Kushner PJ, England MH, Grise KM, Karoly DJ (2011) Signatures of the Antarctic ozone hole in Southern Hemisphere surface climate change. Nat Geosci 4:741–749. doi:10.1038/ngeo1296
van den Broeke MR, van Lipzig NPM (2004) Changes in Antarctic temperature, wind and precipitation in response to the Antarctic Oscillation. Ann Glaciol 39(1):119–126. doi:10.3189/172756404781814654
Wahr J, Molenaar M, Bryan F (1998) Time variability of the Earth's gravity field: hydrological and oceanic effects and their possible detection using GRACE. J Geophys Res 103(B12):30205–30229. doi:10.1029/98JB02844
Wahr JM, Jayne SR, Bryan FO (2002) A method of inferring deep ocean currents from satellite measurements of time variable gravity. J Geophys Res 107(C12):3218. doi:10.1029/2001JC001274
Zhang ZZ, Chao BF, Lu Y, Hsu HT (2009) An effective filtering for GRACE time-variable gravity: the fan filter. Geophys Res Lett 36(17):L17311. doi:10.1029/2009GL039459
Zlotnicki V, Wahr J, Fukumori I, Song YT (2007) Antarctic circumpolar current transport variability during 2003–2005 from GRACE. J Phys Ocean 37:230–244. doi:10.1175/JPO3009.1